Assessing the driving force of a structural distortion by the simulated evolution of the local density of states

Francesca Tavazza,* Valeria Meregalli,† and Leo Miglio
Istituto Nazionale di Fisica della Materia and Dipartimento di Scienza dei Materiali dell'Università di Milano, via Emanueli 15, 20126 Milano, Italy

Massimo Celino
Ente per le Nuove Tecnologie, ENEA, C.R.E. della Casaccia, P.O. 2400, 00100 Roma, Italy
(Received 28 October 1997)

In this paper we show that the driving force leading to the metal-semiconductor structural phase transition occurring in epitaxial $FeSi_2$ with film thickness, originates from a local Jahn-Teller distortion. This effect can be straightforwardly seen by the analysis of the site-projected density of states during a variable cell molecular dynamics for the bulk configuration. We point out that the evolution of the local density of states is a reliable and powerful tool solely provided by tight-binding molecular dynamics. [S0163-1829(99)00905-4]

I. INTRODUCTION

Tight-binding molecular dynamics (TBMD) has been recently adopted for numerical simulations of materials and structures involving group IV elements[1] and III-V compounds.[2] An increasing amount of applications are taking place whenever the complexity or the size of the system prevents the employment of Car-Parrinello first-principles approach. Probably the main reason of its success is related to the low computational cost entailed by the semiempirical estimation of the electronic states entering the attractive (covalent) part of the potential and by the phenomenological description of the repulsive part through two-body functions. Still, no great attention has been payed to the fact that the evolution of the electronic density of states (DOS) can provide important, additional information, especially at a local scale. The latter feature is straightforwardly obtained in the tight-binding (TB) scheme by site projection of the DOS, resulting in a real-space imagining of the electronic features, which is particularly useful in understanding the origin of structural instabilities. This is the case of pseudomorphic $FeSi_2$ in the fluorite structure which evolves into the stable orthorhombic form as the epitaxial film thickness is increased.

The stable form of $FeSi_2$ at room temperature, i.e., the β phase, displays a semiconductive gap of 0.85 eV, and for this reason it has attracted a lot of interest in view of optoelectronic applications in silicon-integrated devices.[3] However, there is a more fundamental reason to study this binary compound since, at variance with respect to the related compounds $NiSi_2$ and $CoSi_2$, the metallic fluorite phase γ- $FeSi_2$ is not bulkstable. Muffin tin orbitals (LMTO-ASA) calculations by Christensen[4] have predicted a high DOS at the Fermi level, suggesting that a Jahn-Teller distortion may drive the cubic structure into the orthorhombic β form, but no description of the actual deformation pattern has been given up to now. Recent molecular beam epitaxy experiments have shown that the γ phase can be stabilized at very low coverage on top Si(111) (pseudomorphic growth), due to the different symmetry of the hexagonal Si lattice and the rectangular orthorhombic projection and the bad lattice parameters matching provided by the β phase, as compared to the superior interface bonding provided by the fluorite arrangement ($a=5.37$ Å).[5] As the film exceeds a few monolayers, a real structural phase transition to the stable form occurs at annealing temperatures which decrease with thickness. It seems very likely that, whatever the distortion pattern, the bonding to the substrate just provides an interface pinning of the fluorite arrangement, with no sizable changes in the electronic features. For this reason we are confident that a molecular dynamics simulation in the bulk configuration can also provide a picture of the actual structural evolution and, in case, a confirmation of the Jahn-Teller origin of the driving force. Since the γ phase is not bulk stable, we should be able to see, even at low temperatures, the spontaneous change in size and shape of the unit cell from cubic to orthorhombic. The latter displays 24 atoms on a base centered lattice. Nevertheless, in our variable-cell TBMD scheme it is better to choose a target structure with 48 atoms in a simple orthorhombic cell ($a=9.86$ Å, $b=7.79$ Å, $c=7.83$ Å),[6] since it can be considered as the natural evolution of one tetragonal parent structure, easily extracted from a cubic supercell of eight conventional CaF_2 units.

In this paper we show that the metal-semiconductor transition does occur with no kinetic barrier in between and that the tight binding potential provides the right target structure which, still, did not enter the parameter fitting. Moreover, the detailed analysis of the site projected density of states shows that the gap is formed in selected sites at different simulation times. This is shown to be generated by a local deformation of the cubic cage of silicon atoms in the fluorite pattern and by the displacement of the iron atom inside, pointing out the symmetry breaking which is typical of the Jahn-Teller effect. The driving force of the structural phase transition occurring with film thickness is therefore local in origin, but a correlated pattern of site distortions is needed in order to achieve the stable orthorhombic structure, in agreement with the phonon softening that comes out from lattice dynamics calculation.[7] The key role played by the occurrence of the

Fermi level on the DOS peak is also demonstrated by the unsuccessful simulated transformation in the case of $CoSi_2$, where the density of states is very similar to $FeSi_2$, but the extra electron per metal atom provides a Fermi level location at higher energies, in a low density region.

II. THE TIGHT BINDING POTENTIAL

Our interatomic potential is essentially the same as the one we used for total energy calculations of the pseudomorphic phases in $FeSi_2$[8,9], FeSi, and CoSi,[10] where a successful prediction of the stability hierarchy have been obtained. It is grounded on the common scheme which divides the total energy into an attractive part E_{bs}, originated by a summation over occupied TB states $\varepsilon_{n,k}$ (n is the band index and k is the wave vector), and a repulsive contribution $E_{\rm rep}$, which is generated by the summation of one short-range, two-body potential $\Phi(r_{ij})$ on the relevant shell of neighbors (j)

$$E = E_{bs} + E_{\rm rep} = \sum_{nk} \varepsilon_{nk} + \sum_{i<j} \Phi(r_{ij}). \tag{1}$$

E_{bs} is usually negative and decreases in magnitude by increasing the lattice spacing, according to the progressive reduction in ε_{nk} dispersion. The latter feature is in turn provided by a Slater-Koster (SK) parametrization of the TB matrix H_{ij},[11] where the the diagonal (onsite $i-i$) elements are fixed, and the dependence of the hopping (intersite $i-j$) elements with $\mathbf{r}_{ij}$ is cast in terms of the director cosines and of the two-centers integrals $V_{l,l',m}(r_{ij})$. The latters are considered as parametric radial functions, where l,l' label the symmetry of the basis orbitals $(s,p,d,\cdots)$ and m the axial symmetry of the molecular orbital formed along the bond $(\sigma,\pi,\delta,\cdots)$. The radial dependence is usually taken to be an inverse power function, where the steepness changes according to the orbitals involved:

$$V_{l,l',m}(r_{ij}) = \eta_{l,l',m}\left(\frac{r_{ij}^0}{r_{ij}}\right)^{n_{l,l'}}. \tag{2}$$

Here $\eta_{l,l',m}$ is the two-centers parameter at the equilibrium interatomic distance r_{ij}^0 in the reference phase. We have found that the Harrison prescription[12] for the actual value of the exponent works fairly well in the case of transition metal silicides: $n_{l,l'}=2$, 3.5, or 5 if none, one, or both orbitals are d like, respectively. However, the decay at large interatomic distances is too slow and a steplike cutoff is usually operated when the reproduction of the *ab initio* bands and DOS is satisfactory up to third neighbors pairs in the case of fluorite $FeSi_2$.

At variance with respect to our previous total energy calculations,[8–10] in molecular dynamics simulations it is compulsory to adopt a smooth cutoff of the interactions (because of energy conservation) and to place it within the global cutoff radius imposed by the size of the simulation cell. Therefore we multiplied both the TB elements and the repulsive interactions $\Phi(r_{ij})$ by

$$\frac{1}{2}\left[1-\sin\left(\frac{\pi}{2}\frac{r-r_c}{w}\right)\right], \tag{3}$$

where $r_c=3.3$ Å and $w=0.3$ Å. Accordingly, below 3 Å the cutoff function is set to 1 and above 3.6 Å it is 0, a choice that excludes Fe-Fe third neighbors pairs at 3.81 Å in fluorite $FeSi_2$. This is a satisfactory compromise which does not alter the stability hierarchy between the γ and the β phases, still allows a limited simulation cell. Moreover, as we will see in the following, it includes some Si-Si and Fe-Fe third neighbors pairs of the target structure, one condition that is crucially important to get a successful structural distortion.

In order to have a reliable description of the electronic features, the TB basis set has to be sufficiently large, and an accurate fitting of the parameters $\eta_{l,l',m}$ has to be performed onto the *ab initio* bands. In particular, we found that a minimal basis set (sp_3) is sufficient for silicon, but an extended one (sd_5p_3) is necessary for the transition metal. In fact, the polarization p states of Fe are located in energy not far from the occupied p ones of silicon and a sizable hybridization is expected. This is also relevant for the flattening of the electronic bands at the Fermi level in fluorite $FeSi_2$, which gives rise to a high density of states. In short, 27 parameters (22 $\eta_{l,l',m}$, plus E_{3s}, E_{3p} for silicon, and E_{3d}, E_{4s}, E_{4p} for iron) have been fitted by a least square minimization to the augmented plane wave (FLAPW) (Ref. 13) electronic bands for the fluorite structure and (CsCl) FeSi, another metallic and pseudomorphic phase (see Ref. 8). In the latter case, Fe-Fe pairs are much closer (second neighbor position, as it happens for a few of them in β-$FeSi_2$) than in the fluorite configuration (third neighbors), and the accuracy in the fitting of the corresponding parameters is greatly improved. Naturally the onsite elements are slightly different between FeSi and $FeSi_2$, due to a different charge transfer produced by the change in stoichiometry. In our simulations (for $FeSi_2$), however, we did not update the onsite elements with atomic displacements, since the variations turned out to be negligible. Therefore, the stable, target phase of our simulation does not enter the fitting procedure, which is based on two bulk unstable structures sufficiently simple for a unique attribution to the first principle bands.

The repulsive term in Eq. (1) phenomenologically represents the quantum-mechanical interaction between occupied orbitals and includes the *a posteriori* correction to the fact that we have kept frozen the diagonal TB elements (a feature which does not take into account the changes in orbital orthogonalization with the atomic positions[14]). It is questionable whether a simple two-body summation can play such a role, still our experience with total energy calculations and molecular dynamics simulations suggests that a simple inverse power law, with the same cutoff radius as the TB hopping elements, gives fairly accurate results:

$$\Phi(r_{ij}) = \Phi_{\alpha,\beta}(r_{ij})^{-m_{\alpha,\beta}}, \quad \alpha,\beta = \text{Si, Fe}. \tag{4}$$

Here the prefactor and the exponent take different values depending on the atomic species involved in the pair potential, and we expect a steeper behavior in the case of iron pairs. These parameters are fitted by stability and equilibrium conditions on to the lattice parameters and the bulk modula of the reference phases. In order to be coherent to the attractive part, we obtained independent values for $\Phi_{\rm Si,Si}$, $\Phi_{\rm Fe,Fe}$, $m_{\rm Si,Si}$, $m_{\rm Fe,Fe}$ from the two lattice constant and the two FLAPW bulk modula of γ-$FeSi_2$ and (CsCl)-FeSi,[13] whereas

$\Phi_{\mathrm{Fe,Si}}$ and $m_{\mathrm{Fe,Si}}$ enter the stability and equilibrium conditions as a geometric and an arithmetic average, respectively, of the corresponding values for the homonuclear pairs.[8] We note that the exponent in Eq. (4) is roughly the double of the effective value for the corresponding TB elements, according to what is predicted for the orthogonality corrections discussed above and very clearly explained in Ref. 14.

The forces entering the molecular dynamics simulation have been calculated by a straightforward derivative of the repulsive potential and a Hellman-Feynman estimation of the attractive part, retaining only $k=0$ terms:[2]

$$F_{i,x}^{bs}=-2\sum_{n,k} f_{n,k}\frac{\partial}{\partial r_{i,x}}\langle n,k|H|n,k\rangle$$
$$=-2\sum_{n,k}\sum_{l',j'}\sum_{l,j} f_{nk}C^{*}_{l'j'}(nk)C_{lj}(nk)\frac{\partial}{\partial r_{i,x}}H_{l'j',lj}(k). \tag{5}$$

Here i,x indicates the atom and the Cartesian component, respectively, f is the Fermi function, and $C_{lj}(nk)$ are the eigenvectors of the Fourier transformed TB matrix $H_{l'j',lj}(k)$.

III. THE *NPT* MOLECULAR DYNAMICS

A. The Parrinello-Rahman algorithm

The usual MD simulation, in the *NVE* ensemble, is based on the numerical integration of the dynamical equations derived by the following Lagrangian:

$$\mathcal{L}_0=\sum_{i=1}^{N}\frac{m_i}{2}(\dot{\mathbf{r}}_i)^2-E(\{\mathbf{r}_i\}), \tag{6}$$

where $E(\{\mathbf{q}_i\})$ is the interaction potential of the N particles of mass m_i that compose the system. The total energy of the atomic system

$$T+E=\sum_{i=1}^{N}\frac{m_i}{2}(\dot{\mathbf{r}}_i)^2+E(\{\mathbf{r}_i\}) \tag{7}$$

is a conserved quantity during the dynamical evolution of the system.

As showed by Parrinello and Rahman,[15] a time-dependent metric tensor G describing the simulation cell can be introduced to allow volume and shape variations with time:

$$G=h^t h. \tag{8}$$

Here, the matrix $h=(\mathbf{a},\mathbf{b},\mathbf{c})$ contains the components of the vectors $\underline{a}$, $\underline{b}$, $\underline{c}$ which define the simulation cell. In this way the particles positions can be obtained in term of scaled coordinates s_i, and the MD cell volume is given by

$$V=\mathbf{a}\cdot(\mathbf{b}\times\mathbf{c})=\det h. \tag{9}$$

When the size and shape of the simulation cell is allowed to vary at fixed external pressure P_{ext} the Lagrangian (6) turns into

$$\mathcal{L}_1=\sum_{i=1}^{N}\frac{m_i}{2}(\dot{\mathbf{s}}_i^t G\dot{\mathbf{s}}_i)-U(\{\mathbf{r}_i\})+\frac{W}{2}\mathrm{Tr}(\dot{h}^t\dot{h})-P_{\mathrm{ext}}V, \tag{10}$$

where W is the mass of an ideal piston which sets the external pressure. The time variation of h is determined by the imbalance between the latter and the instantaneous value of the internal stress.

The (constant) energy of the system+environment is then

$$\sum_{i=1}^{N}\frac{1}{2m_i}(\mathbf{p}_i)^2+E(\{\mathbf{r}_i\})+\frac{W}{2}\mathrm{Tr}(\dot{h}^t\dot{h})+P_{\mathrm{ext}}V. \tag{11}$$

It can be shown that the Lagrangian $\mathcal{L}_1$ generates an isoenthalpic, isobaric dynamics, apart from a small correction arising from the term W.[15]

Finally, it is worth spending some time on the choice of W, which plays a relevant role in determining the dynamical properties of the system. By increasing the value of W the volume fluctuations get slower and slower so that, in the limit of very large W, the simulation becomes numerically impractical. Still, in our case it has to be taken sufficiently large in order to counterbalance the fast, nonergodic evolution generated by the large free energy difference between γ and β. Andersen has provided a physical criterion for the choice of W.[16] One can imagine that the MD cell is a portion of a much larger system. The relaxation time $\bar{t}$ of this small subsystem, when disturbed by local imbalances in the pressure, is of the order of $\bar{t}\sim L/c$, where L is the MD cell side and c is the sound velocity. By properly tuning W it is possible to obtain a relaxation time of the MD cell which is close to $\bar{t}$. In our case $L\sim 10$ Å and $\bar{t}\sim 0.5$–1.0 psec, which corresponds to 2–5000 time steps with $\tau=0.2$ fsec, as we were forced to use for the sake of energy conservation. This, in turn, means that the transformation takes place within 5000 τ if $W=10^4$ amu.

B. The Nosé algorithm

A constant-temperature system is usually surrounded by a heat reservoir. In the Nosé formulation[17,18] it is described by only one extra degree of freedom s to be included in the Hamiltonian of the system. This is done by adding one potential and one kinetic energy term, which depend on s and its conjugate momentum, respectively. More in detail, a set of virtual variables are introduced (coordinate $\mathbf{r}_i$, momentum $\mathbf{p}_i$, and time t) which are related to the real variables $(\mathbf{r}_i,\mathbf{p}_i',t')$ by

$$\mathbf{r}_i'=\mathbf{r}_i,\quad \mathbf{p}_i'=\frac{\mathbf{p}_i}{s},\quad t_i'=\int\frac{dt}{s}. \tag{12}$$

The real velocity $(d\mathbf{r}_i'/dt')$ is therefore obtained via a scaled form of the virtual velocity

$$\frac{d\mathbf{r}_i'}{dt'}=s\frac{d\mathbf{r}_i'}{dt}=s\frac{d\mathbf{r}_i}{dt}. \tag{13}$$

The (constant) energy of the system+heat reservoir can be written in terms of the variable s and the virtual variables of the system as follows:

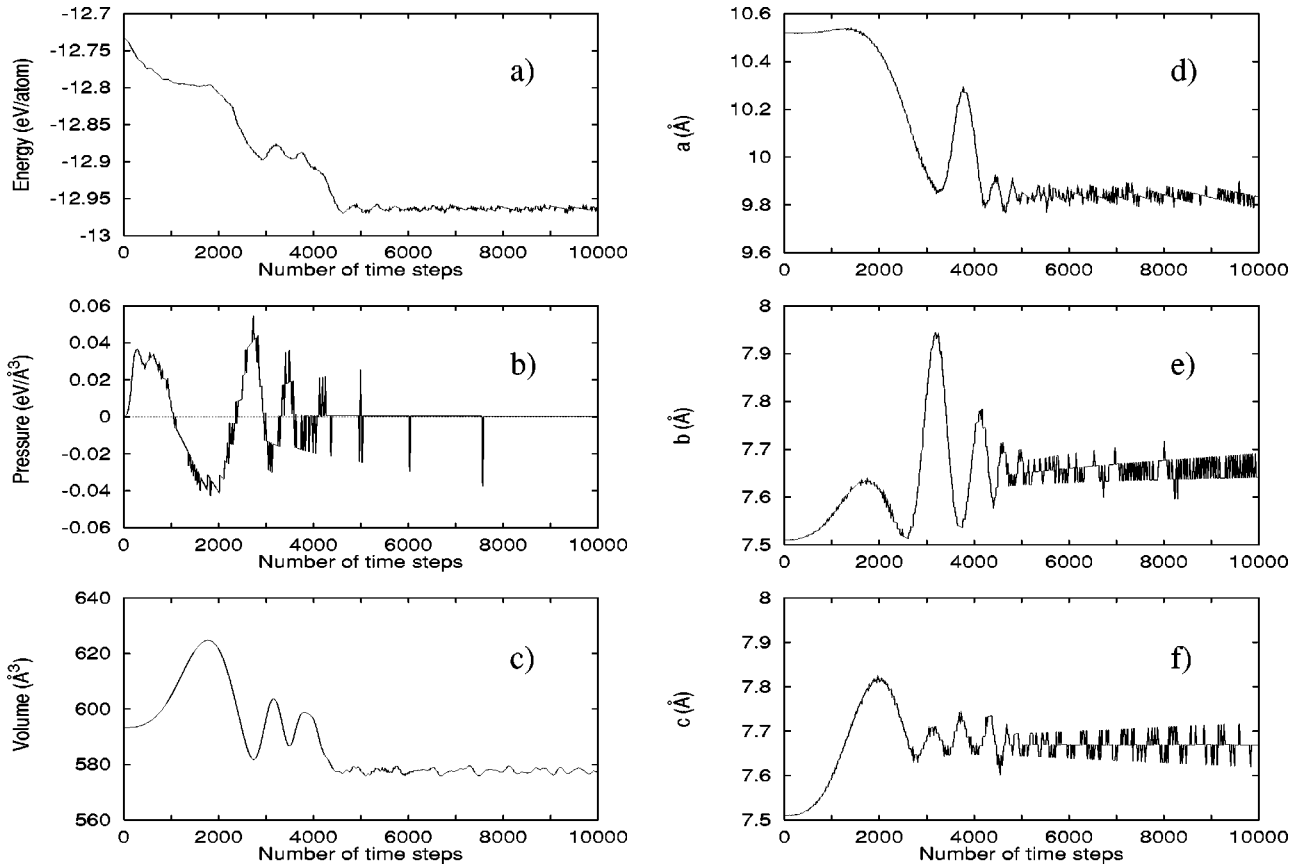

FIG. 1. Instantaneous evolution in time within the first 10 000 time steps of system energy, pressure, volume, and cell sides.

$$\sum_{i=1}^{N} \frac{\mathbf{p}_i^2}{2m_i s_N^2} + E(\{\mathbf{r}_i\}) + \frac{p_s^2}{2Q} + gK_B T_{\text{ext}} \ln s, \qquad (14)$$

where p_s is the conjugate momentum of s, T_{ext} is the external temperature, and g is practically equal to the number of degrees of freedom of the system. Q is a parameter with the dimensions of energy $\times(\text{time})^2$ and acts as a mass for the motion of s. In particular, if Q has a large value then the energy flow is slow, leading to adiabatic dynamics for $Q \rightarrow \text{inf}$. The reverse is true if Q is very small, but the energy oscillates, resulting in equilibration problems. Since we set $T_{\text{ext}}=100$ K and since the system has to dissipate some 0.15 eV/atom in E when moving from γ-$FeSi_2$ to β-$FeSi_2$, a very small value of Q would be desiderable, but for the stability energy problems. Therefore we used a ''standard'' value of 50 $Å^2$/amu, but we included a velocity rescaling algorithm for fluctuations in temperature exceeding the 80–120 K range. Obviously this is brute force method that turned out to be adequate only by the *a posteriori* analysis of our results.

C. The *NPT* equations

The final expression for the Lagrangian governing the time evolution of the extended system at constant pressure, constant temperature and variable cell shape is

$$\mathcal{L} = \sum_{i=1}^{N} \frac{m_i}{2} s_N^2 \dot{s}_i G \dot{s}_i - U(\{\mathbf{r}_i\}) + \frac{W}{2} \text{Tr}(\dot{h}^t \dot{h}) - P_{\text{ext}} V + \frac{M_s}{2} \dot{s}^2 - gKT_{\text{ext}} \ln s. \qquad (15)$$

It is a function of the ''virtual'' variables $\{\mathbf{s}_i, h_{\alpha\beta}, s\}$ and of their time derivative with respect to a ''virtual'' time t.

Thus, two kinds of coordinates frames are introduced: the scaled frame and the real frame. The use of the periodic boundary condition and the integration of the equation of motion are carried in the scaled frame. On the other hand, the calculation of the TB forces, energy and other structural data are carried out in the real frame.

The equations derived from this Lagrangian are integrated by a predictor-corrector method[19,20] as the force terms are here dependent upon the actual velocity as well. In particular, we have used the integration algorithm up to fifth order in the case of the second order equations, in order to improve the energy conservation. In should be noted, in fact, that the integration with velocities dependent force terms is less accurate than the usual velocity independent case.

IV. RESULTS

A simulation of 93 000 τ was performed, but the transformation from γ to β structure took place in the first 5000τ according to the ''physical'' relaxation time of our simulation cell. For this reason Fig. 1 displays the instantaneous evolution of energy, pressure, volume, and sides of the simulation cell only during the first 10 000τ, in order to make more evident what occurs during the structural transformation. It is possible to note meaningful variations only in the first 5000τ, until they reach convergence values that remain unchanged during the rest of the simulation.

The simulation cell is initially taken as the tetragonal

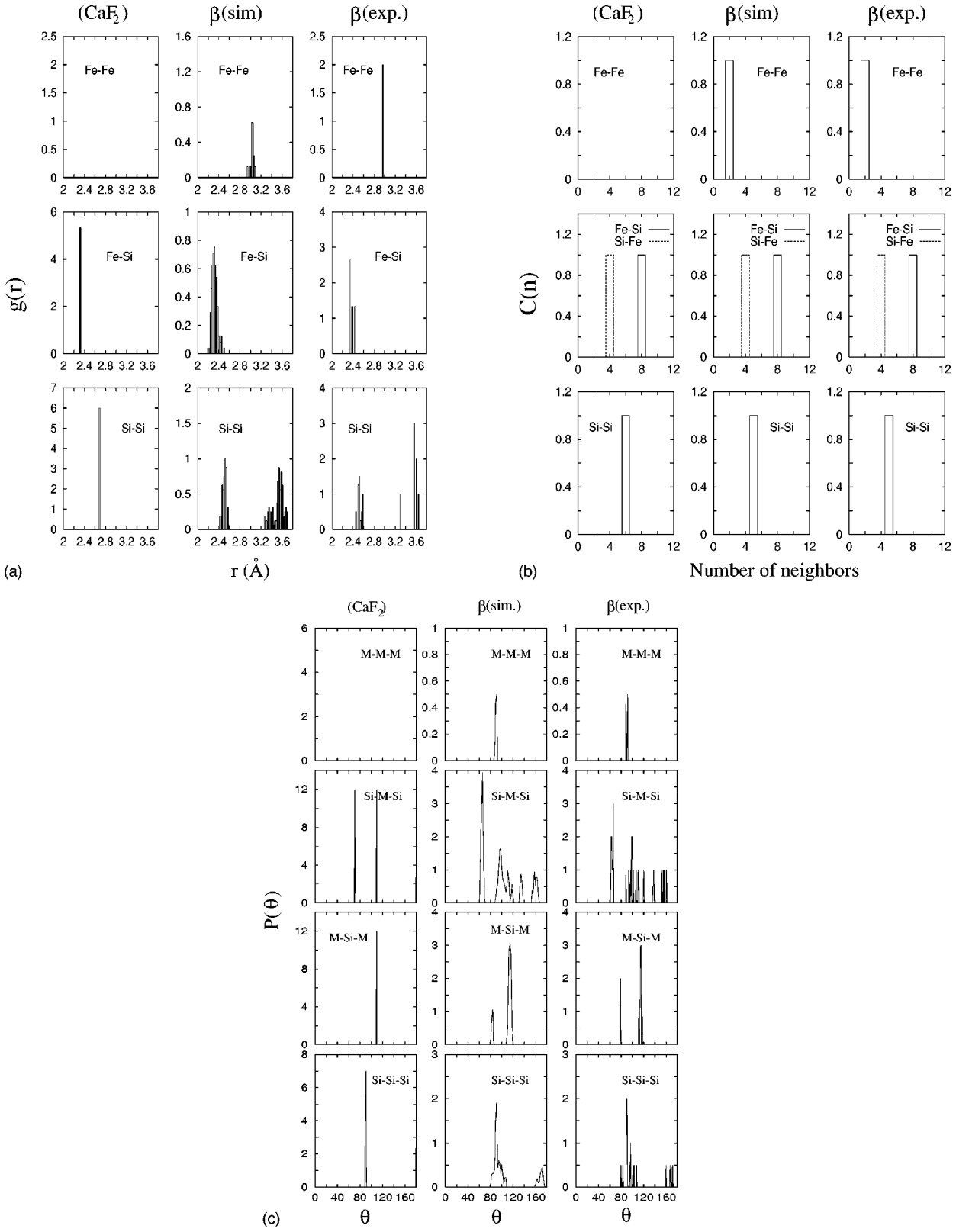

FIG. 2. Pair distribution $g(r)$ (a), bond-angle distribution $P(\theta)$ (b), and site-coordination function $c(n)$ (c) for ''gamma'' (left), beta (center), and simulated (right) structures. The site-coordination function has been evaluated for pairs within 3.2 Å and shows how the simulated structure is orderly coordinated according to the crystalline beta phase, both at first and second neighbors (1.0=100).

nucleus (x oriented) of a cubic supercell made by 8 fcc units, where a is twice the fcc edge and $b=c$ are the diagonals of the fcc square faces (10.74, 7.59, 7.59 Å). Then, for simulational reasons, the actual starting cell (10.52, 7.51, 7.51 Å) is obtained by minimizing the cohesive energy with respect to a and b variations at fixed atomic configuration. Such a cell contains 48 atoms and, as the simulation evolves, transforms into the orthorhombic cell by decreasing a and increasing b

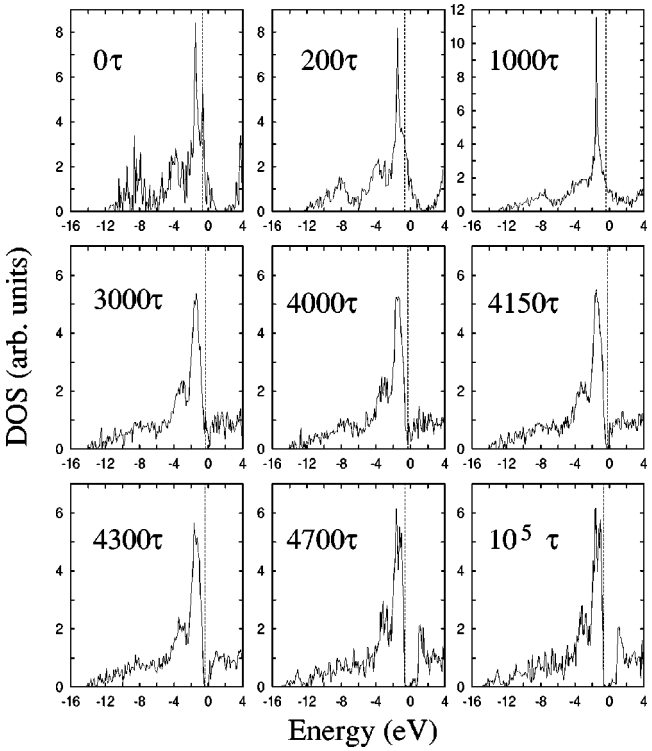

FIG. 3. Evolution in time of the electronic DOS during the simulation. The DOS are taken by considering $27k$ points in the Brillouin zone, as well as atomic positions averaged over 50τ around the number of time steps displayed in the panels.

and c ($a=9.82$, $b=7.65$, $c=7.67$ Å, as taken at 5000τ) fairly close to the experimental values.

By observing the pair distribution $g(r)$, the bond-angle distribution $P(\theta)$, and the site-coordination function $c(n)$ displayed in Figs. 2(a)–2(c), one can see that the main difference between the initial structure γ (or CaF_2) and the target (β experimental) is in the secondary coordination. The β phase, in fact, has Si-Si second neighbors fivefold coordinated, at variance to what happens in γ-$FeSi_2$ where they are sixfold coordinated. Moreover, the former contains Fe-Fe and Si-Si third neighbors pairs at closer interatomic distance (<3.6 Å) and we noticed that no structural distortion occurs for a cutoff function completely excluding these interactions. With respect to the first neighbors coordination

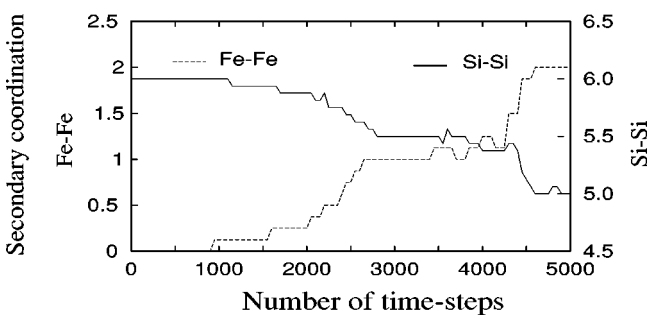

FIG. 4. Evolution of the average secondary coordinations for Fe and Si sites, Fe-Fe and Si-Si pairs, respectively. There is essentially a two-step behavior for both sites, such that after the first step (from 2000 to 2700τ) the values are exactly half way between those of the γ and β phases.

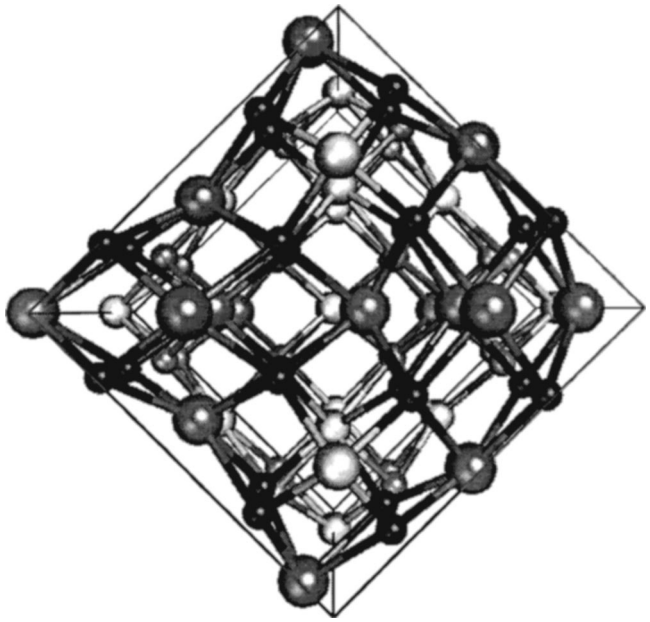

FIG. 5. Simulation cell at 3000τ. As can be seen the spatial distribution of the site transited Fe (large, dark balls) and Si (black, small balls) atoms follows a very regular pattern.

Fe-Si, Si-Fe, there is a sizable difference between the two phases only in the bond-angle distribution; the pair distribution and the site-coordination remaining roughly unchanged in passing from one structure to the other. The latter are evaluated for atomic pairs within 3.2 Å, in order not to mix second and third neighbors shells. In the central column of each panel (a)–(c) are reported the final results of our simulation (β simulated), taken for the average positions over the last 50τ. As it appears from the figure, the final atomic positions inside the simulation cell agree very well to the ex-

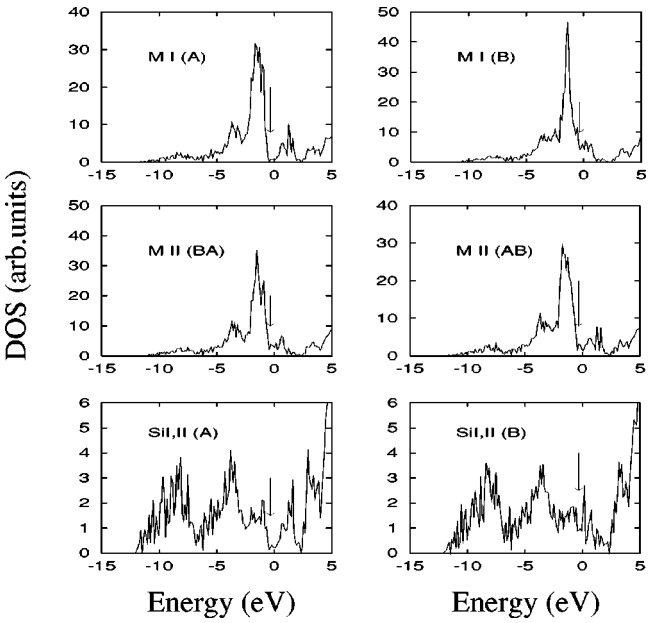

FIG. 6. Site projected DOS at 3000τ. The sites are labeled with respect to the final crystallographic position in the β structure (metal I, metal II, silicon I, and silicon II) and to the local gap opening (A=occurred, B=nonoccurred, AB, BA=in between).

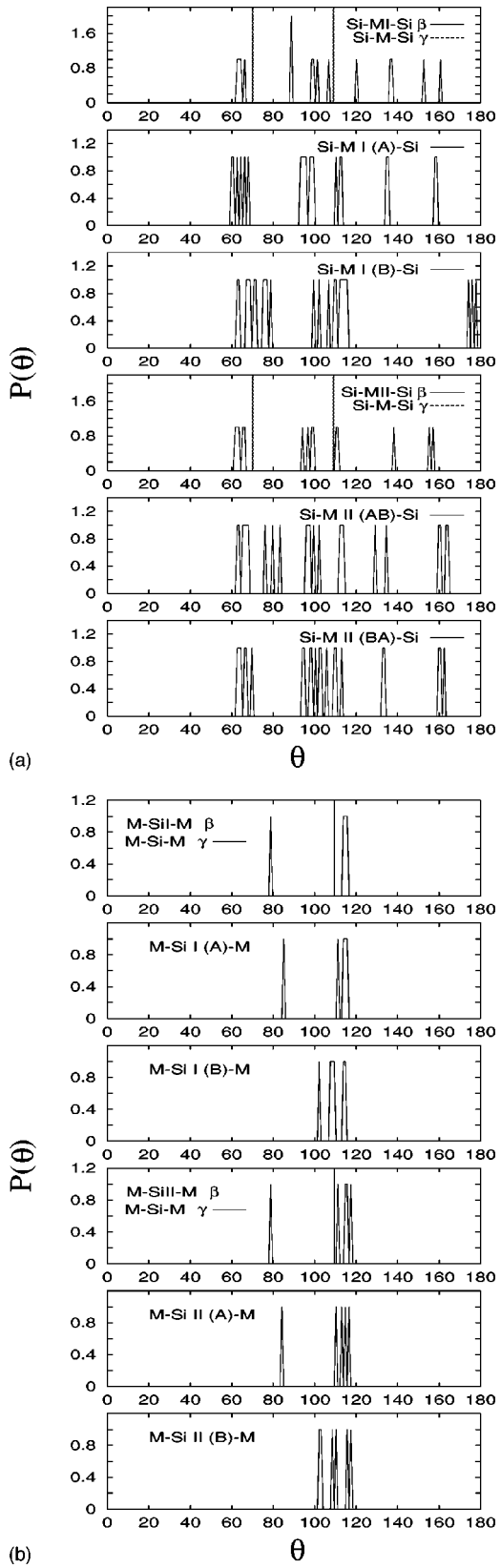

FIG. 7. Bond-angle distribution at 3000τ, with respect to FeI, FeII, SiI, SiII pivot atoms. For each case it is displayed one representative distribution of the different found local environment. By $\underline{A}$ we indicate a β-like site, by $\underline{B}$ a γ-like site, and by AB or BA one that is half way, having $\underline{A}$ first if the pivot atom has a β-like secondary coordination.

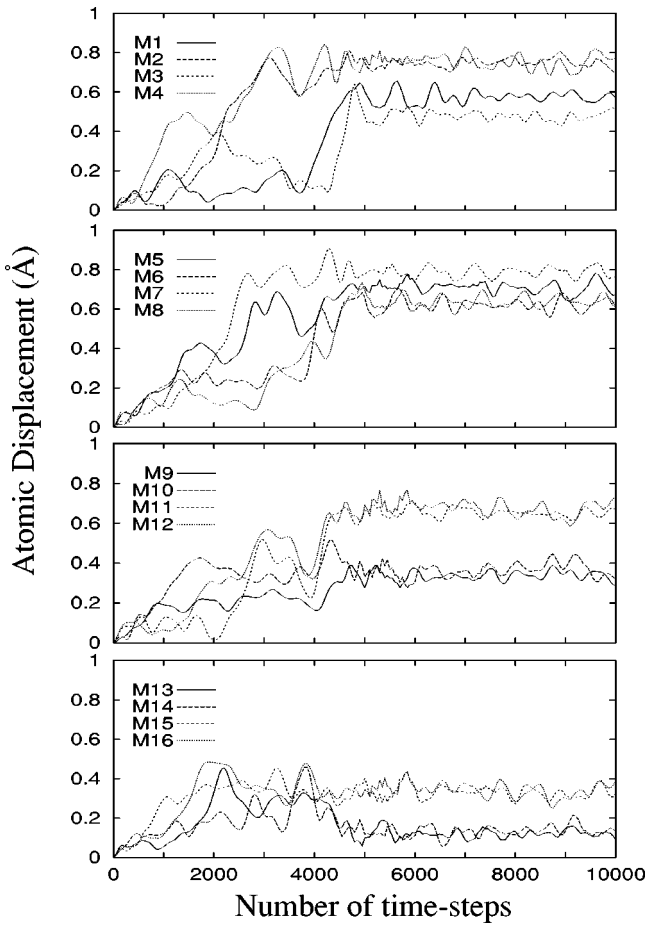

FIG. 8. Individual displacements (in modulus) of the iron atoms during first 10 000 time steps of the simulation.

perimental target structure. This result, together with the rather good values obtained for the cell sides, guarantees that the structure achieved at the end of the simulation is actually a β structure. Because the simulation was performed at very low temperature ($T=100$ K), we can conclude that the structural deformation does occur with no kinetic barriers inbetween, as predicted in the static calculation of Ref. 8.

It is possible to follow the evolution of the metal-semiconductor transition by the electronic DOS changes with simulation time (Fig. 3), which also provides global information on the structural evolution. The DOS reported in Fig. 3 are taken by considering 27 k points in the Brillouin zone, as well as atomic positions averaged over 50τ around the number of time steps displayed in the panels. It is possible to note that, after the initial disappearance of the sharp density peak at the Fermi energy ($0-200\tau$) as a consequence of the thermal symmetry breaking, a spread out of low-energy s states begins, and it is completed at 3000τ. In the meantime the main peak at -1.58 eV, corresponding to nonbonding d metallic states is progressively enhanced and sharpened, showing that a Si-Fe bond breaking is occurring, that produces a sizable lowering of the DOS at E_f. This phenomenon reaches its maximum at 1000τ, and reverses after that time, so that at 3000τ there is a sizable pd bonding again but E_f remains in a low-DOS position. This indicates that a new structural configuration has occurred in passing from 1000 to 3000τ. Between 3000τ and 4000τ there is no apparent

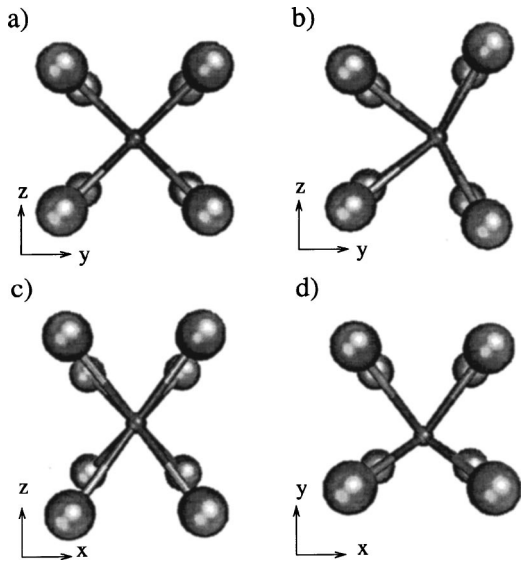

FIG. 9. Top and side views (b)–(d) of the distorted cubic cage of Si around the metal site, as extracted by the central part of our simulation cell at 3000τ. In (a) the original cubic arrangement is shown.

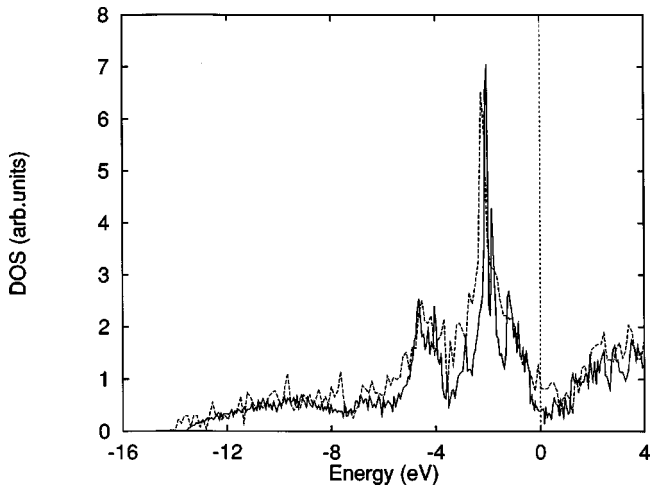

FIG. 10. DOS for $CoSi_2$ at the beginning (solid line) of the simulation and after $35\,000\tau$ (dashed line).

change in the DOS, but at 4150τ the gap opening sets in and the metal-semiconductor transition is completed at 4700τ. The DOS does not change any more after that time, showing the same shape and gap size of the *ab initio* results reported in Ref. 4. Looking at the energy and volume curves versus time again (Fig. 1), it is interesting to note that the energy lowering occurs in three different steps: the first between 0 and 2000 τ, the second one centered at 2500τ, and the last between 4000 and 4700 τ. The analysis of the DOS and volume evolution allows us to interpret this sequence as corresponding to a (anti)-bond-breaking volume expansion first (the initial step), and to two bond-forming volume contractions afterwards. In particular the third step is related to the gap opening.

A more detailed analysis of the configurational path during the first 5000τ illustrates how the gap opening occurs and whether a true Jahn-Teller distortion takes place. In Fig. 4 is displayed the evolution of the average secondary coordinations for Fe and Si sites, Fe-Fe, and Si-Si pairs, respectively. This is structurally meaningful since, as we pointed out before, the primary coordination of Fe and Si remains unchanged in going from the γ to the β structure. There is essentially a two-step behavior for both sites, such that after the first step (from 2000 to 2700 τ) the values are exactly half way between those of the γ and β phases [see Fig. 2(b)]. The transformation is completed in a second, separate step inbetween 4000 and 4700 τ. It also matches very well to the steps pointed out by DOS, energy, and volume evolutions. The interesting point is to understand whether each step corresponds to a cooperative motion at all atomic sites leading to the target configuration just in the second one, or if a complete transformation is obtained at a local scale in different times for different sites. To this end the evolution of the secondary coordination for each Fe and Si was studied, as well as the site-projected DOS at 3000τ, i.e., between the first and the second step.

We noted that at 3000τ half of the iron and the silicon atoms display the same number of neighbors as it would have in the β phase. The remaining atoms, on the contrary, have the same secondary coordination as at the very beginning of the simulation. In particular, Fig. 5 shows that the spatial distribution of the site transited Fe (large, dark balls) and Si (black, small balls) atoms follows a very regular pattern, pointing out the correlation existing among the local distortions.

However, we still do not know if a local gap opening occurs as a consequence of the lattice distortion, but we can look at the site projected DOS at 3000τ for an answer. In Fig. 6 we show our results by labeling the sites with respect to the final crystallographic position in the β structure (metal I, metal II, silicon I, and silicon II) and to the local gap opening (A = occurred, B = nonoccurred, AB, BA = in between). Both SiI and SiII sets, 16 atoms in each one for our 48-atoms simulation cell, are sharply subdivided into two classes of eight atoms each: one corresponds to β-like projected DOS and contains only atoms with β-type secondary coordination (label A in Fig. 6), the other is related to completely fluorite type atoms, with fluoritelike DOS (label B in Fig. 6). Four FeI atoms out of eight do display a gap, and their secondary coordination is entirely of β-type (label A). The remaining four atoms are essentially fluoritelike (label B) and no local gap is present in their DOS. All eight FeII sites are in an intermediate stage for what concerns the DOS, but four of them show a β-like secondary coordination (AB), while the other four have a γ-like one (BA). The vertical arrow indicates the position of E_f for each representative panel. From this analysis it is concluded that the gap opening is not straightforwardly related to the secondary coordination variation, as it could be supposed on the basis of simple arguments, such as Fig. 4, and of the fact that the difference in the two structures is actually greater for the secondary coordination than for the primary. Obviously all the features of the atomic projected DOS can be completely explained by considering the modifications bond angles in the first-neighbors shell.

We report in Figs. 7(a), 7(b) the bond-angle distribution at 3000τ, with respect to FeI, FeII, SiI, SiII pivot atoms (Si-FeI-Si, Si-FeII-Si, Fe-SiI-Fe, and Fe-SiII-Fe). For each case we display one representative distribution of the differ-

ent local environment that we found (i.e., the bond angles with next neighbors). By A we indicate a β-like site, by B a γ-like site, and by AB or BA a half way one, having A first if the pivot atom has a β-like secondary coordination. It turns out that all the atoms with first-neighbors bond angles definitely pertaining to one kind (β- or γ-like) also have secondary coordination of the same kind. As it is displayed in Figs. 7(a), 7(b) FeI, SiI, and SiII behave this way. On the contrary, FeII behave at variance, having bond-angle configurations only partially transformed in agreement to the projected DOS. The sharp partition of FeI at 3000τ into γ type or β type is also evident in the first two panels of Fig. 8, where the individual displacements (in modulus) for the corresponding eight atoms are shown. The converse is true for FeII (two bottom panels), where the situation is settled just at the second step ($4150-4700\ \tau$).

In Fig. 9 we display the top and side views (b)–(d) of the first-neighbors cluster around the metal site for the distorted structure, with respect to the original cubic arrangement (a), as extracted by the central part of our simulation cell at 3000τ. We see that a displacement of Fe towards one of the cube faces occurs, that generates a bond angle distortion at first neighbors. This, in turn, gives rise to a deformation of the silicon cage which ends up in a solid with two square faces of different side and four nearly regular trapezoidal faces. This is prototypical of β-$FeSi_2$ and of Jahn-Teller distortions in general. Therefore local symmetry breaking generates a local gap opening but the site distortions are somehow correlated in a pattern that we believe to be independent of the choice of our simulation cell.

In order to demonstrate that a global instability condition has to be fulfilled for this kind of transition to occur, the same simulation has been performed for $CoSi_2$, which is stable in the fluorite structure. In this calculation we have used a tight-binding potential fitted for cobalt silicides, as reported in Ref. 10. Actually the shape of the γ-$CoSi_2$ DOS is very similar to γ-$FeSi_2$ one, but for the Fermi level position which now lies at higher energies, as due to the extra electron per cobalt atom. This shift puts the Fermi level in a low density region, on the contrary of what happens in fluorite $FeSi_2$, where it is superimposed to a high density peak. As can be easily seen in Fig. 10, in this simulation the sample remained essentially in the initial configuration and no transition is observed for $35\,000\tau$. This result is therefore completely consistent with the fact the γ-$CoSi_2$ is a stable phase, and allows us to relate the occurring of the transition to the instability due to the Fermi level position in the γ-$FeSi_2$.

V. CONCLUSIONS

Our work demonstrates the reliability and the utility of TBMD in investigating the relations between the structural deformations and the changes in the electronic features during a simulation, where the latter provides the driving force. We believe that this is a performance well beyond the capabilities of other semiempirical methods, and that the possibility of an easy interpretation of the main physical aspects provided by a wise parametrization and by the local analysis of electronic features shows that TBMD can be complementary to first principles techniques even in the case of relatively small simulation cells.

*Present address: Center for Simulational Physics, Dept. of Physics and Astronomy, The University of Georgia, Athens, GA 30602-2451.

†Present address: Max-Plank-Institute für Festkörperferschung, Heisenbergstrasse 1, D-70569 Stuttgart, Germany.

[1] C. Z. Wang, K. M. Ho, and C. T. Chan, Comput. Mater. Sci. **2**, 93 (1994), and references therein.

[2] C. Molteni, L. Colombo, and L. Miglio, Europhys. Lett. **24**, 659 (1993); Phys. Rev. B **50**, 4371 (1994); J. Phys.: Condens. Matter **6**, 5243 (1994); **6**, 5255 (1994).

[3] D. N. Leong, M. A. Harry, K. J. Reeson, and K. P. Homewood, Appl. Phys. Lett. **68**, 1649 (1996); Nature (London) **387**, 686 (1997).

[4] N. E. Christensen, Phys. Rev. B **42**, 7148 (1990).

[5] H. von Kaenel, R. Stalder, H. Sirringhaus, N. Onda, and J. Henz, Appl. Surf. Sci. **53**, 196 (1991); A. L. Vazquez de Parga, J. De la Figuera, C. Ocal, and R. Miranda, Europhys. Lett. **18**, 595 (1992); Le Thanh Vinh, J. Chevrier, and J. Derrien, Phys. Rev. B **46**, 15 946 (1992); H. Ch. Schaefer, B. Roese, H. Moritz, A. Rizzi, B. Lengeler, H. Luth, and D. Gerthsen, Appl. Phys. Lett. **62**, 2271 (1993).

[6] Y. Dusausoy, J. Protas, R. Wandji, and B. Roques, Acta Crystallogr., Sect. B: Struct. Crystallogr. Cryst. Chem. **27**, 1209 (1971).

[7] S. Sanguinetti, C. Calegari, V. R. Velasco, G. Benedek, F. Tavazza, and L. Miglio, Phys. Rev. B **54**, 9196 (1996).

[8] L. Miglio and G. Malegori, Phys. Rev. B **52**, 1448 (1995).

[9] L. Miglio, F. Tavazza, and G. Malegori, Appl. Phys. Lett. **67**, 2293 (1995).

[10] H. von Kaenel, C. Schwarz, S. Goncalves-Conto, E. Mueller, L. Miglio, F. Tavazza, and G. Malegori, Phys. Rev. Lett. **74**, 1163 (1995).

[11] J. C. Slater and G. F. Koster, Phys. Rev. **94**, 1498 (1954).

[12] W. A. Harrison, *Electronic Structure and the Properties of Solids* (Freeman, San Francisco, 1980).

[13] K. A. Maeder, H. von Kaenel, and A. Baldereschi, Phys. Rev. B **48**, 4364 (1993).

[14] J. A. Majewski and P. Vogl, in *The Structure of Binary Compounds*, Vol. 2 of *Cohesion and Structure Series*, edited by F. R. de Boer and D. G. Pettifor (North Holland, Amsterdam, 1989), p. 287.

[15] M. Parrinello and A. Rahman, J. Chem. Phys. **76**, 2662 (1982); L. W. Woodcook, Chem. Phys. Lett. **10**, 257 (1971); W. G. Hoover, A. J. C. Ladd, and B. Moran, Phys. Rev. Lett. **48**, 1818 (1982); D. J. Evans, J. Chem. Phys. **78**, 3297 (1983).

[16] H. C. Andersen, J. Chem. Phys. **72**, 2384 (1980).

[17] S. Nosé and M. L. Klein, Mol. Phys. **50**, 1055 (1983); S. Nosé, *ibid.* **52**, 255 (1984); J. Chem. Phys. **81**, 511 (1984).

[18] W. G. Hoover, Phys. Rev. A **31**, 1695 (1984); W. G. Hoover, in *Molecular Dynamics*, Vol. 258 of *Lecture Notes in Physics* (Springer-Verlag, Berlin, 1986).

[19] C. W. Gear, *Numerical Initial Value Problems in Ordinary Differential Equations* (Prentice-Hall, Englewood Cliffs, NJ, 1971).

[20] M. P. Allen and D. J. Tildeley, *Computer Simulation of Liquids* (Clarendon, Oxford, 1987).